

PHYSICS CONTRIBUTION

INVESTIGATIONS OF A MINIMALLY INVASIVE METHOD FOR TREATMENT OF SPINAL MALIGNANCIES WITH LINAC STEREOTACTIC RADIATION THERAPY: ACCURACY AND ANIMAL STUDIES

PAUL M. MEDIN, PH.D.,* TIMOTHY D. SOLBERG, PH.D.,* ANTONIO A.F. DE SALLES, M.D., PH.D.,[†]
CHRISTOPHER H. CAGNON, M.S.,[‡] MICHAEL T. SELCH, M.D.,* J. PATRICK JOHNSON, M.D.,[†]
JAMES B. SMATHERS, PH.D.,* AND ERIC R. COSMAN, PH.D.[§]

Departments of *Radiation Oncology and [‡]Radiological Sciences, and [†]Division of Neurosurgery, University of California Los Angeles, Los Angeles, CA; [§]Department of Physics, Massachusetts Institute of Technology, Boston, MA

Purpose: A new method for stereotactic irradiation of spinal malignancies is presented, with evaluations of the theoretic and practical limitations of localization accuracy and the implementation of the method in swine.

Methods and Materials: In a percutaneous procedure, a minimum of three small (1.7-mm-diameter) titanium markers are permanently affixed to a vertebra. Markers are localized on biplanar radiographs while isocenter positions are determined on CT. An external fiducial frame defines a three-dimensional coordinate system through the patient. Radiographs coupled with a rigid body rotation algorithm account for daily differences in patient position. Phantom studies were used to verify theoretic uncertainty calculations from a simulation program. A swine model was used to evaluate the difficulty and duration of the implant technique, the suitability of the vertebral process as an implant site, vertebral motion due to normal respiration, and the ability to target one vertebra with markers in an adjacent vertebra.

Results: Theoretic accuracy studies confirmed that localization accuracy is a function of marker separation. Phantom studies involving 296 measurements showed that individual implants could be localized within ± 0.25 mm. The largest targeting error observed in 3,600 measurements of 100 implant configurations was 1.17 mm. The implant procedure took 5–10 minutes per site. No significant migration of implants was observed up to 35 days postimplantation, and respiratory motion had no detectable influence on vertebral position. Adjacent vertebrae may be useful for targeting one another with a small sacrifice in localization accuracy.

Conclusions: The use of implanted markers for localization of spinal malignancies has potential for applications in stereotactic radiotherapy. Phantom measurements suggest that localization accuracy similar to intracranial stereotactic radiotherapy techniques is achievable. Swine studies suggest that the implant technique is expedient and feasible for tumor targeting purposes. © 2002 Elsevier Science Inc.

Spine, Stereotaxis, Accuracy, Radiosurgery, Extracranial.

INTRODUCTION

Tumors of the spine affect a large number of people. New cancer patients number 965,000 per year, and skeletal involvement develops in a significant number (1). Unfortunately, the vertebrae are the most common site in the skeletal system for metastases to appear. In a study of 2,000 patients who died of cancer with bone metastases, 69% had vertebral involvement (2). Spinal cancer patients present most often with localized pain. As spinal tumors grow, they cause incapacitating pain, sensory and motor deficits, loss of sphincter function, and vertebral collapse. Reports estimate that 5–10% of all cancer patients eventually have symptomatic epidural compression due to spinal column metastases

(3–5). Primary tumors also involve the spine, but metastatic cancer is much more common. In the case of metastatic cancer, treatment is usually palliative, with the goals of pain relief, elimination of narcotics, improved mobility, and arrest of local tumor growth. Primary tumors can be treated curatively with radiation, surgery, and chemotherapy.

External beam radiation therapy is an effective treatment for the palliation of skeletal metastases. Many clinical studies have been performed to quantify the results of spinal irradiation, but the results are difficult to summarize, because of a wide variety in treatment regimens and in the definitions of success (5–7). In a series of 345 patients, Sorensen *et al.* reported that 79% of ambulatory patients remained ambulatory, 21% of nonambulatory paraplegics

Reprint requests to: Paul M. Medin, c/o Tim Solberg, 200 UCLA Medical Plaza, Suite B265, Los Angeles, CA 90095. Tel: (310) 206-8782; Fax: (310) 794-9795; E-mail: solberg@radonc.ucla.edu

This research has been funded by grants from the North American Spine Society and the University of California Cancer Re-

search Coordinating Committee. Radionics, Inc. of Burlington, MA provided some hardware.

Received Feb 12, 2001, and in revised form Oct 29, 2001. Accepted for publication Nov 8, 2001.

gained ability to walk, and 6% of paralytics regained walking ability (8). In a series of 209 evaluated patients, Maranzano and Latini reported 82% response to back pain, 76% recovery or preservation of walking ability, and 44% improvement in sphincter function (9). In general, 80–90% of patients experience at least some pain relief. In the case of a single-site metastasis, a high dose of radiation may render the patient disease-free for an extensive period of time (1).

Frequently, symptoms recur after radiation therapy. Tong *et al.* reported a relapse rate of 22% in 6 months (7). Gilbert *et al.* found that 55–65% of patients had sustained relief up to 1 year or death (10). Radiation doses to targets in close proximity to the spine are limited by the radiosensitivity of the spinal cord. Excessive radiation to the spinal cord results in transient or permanent myelopathy. The threat of medical and legal complications from radiation-induced myelopathy often results in compromised treatment to keep the spinal cord within “safe” limits (11). The dose–response curve for adverse cord effects begins to rise quickly beyond 50 Gy. A 50-Gy dose is considered safe, with an incidence of myelopathy less than 0.5% (11). Estimated incidence of myelopathy increases to 5% at 57 Gy and 50% at 68 Gy when traditional fractionation schemes (1.8–2 Gy/fraction, 5 fractions/week) are used (12). Once the spinal cord has reached its dose limit, and relapse occurs, reirradiation using conventional external beam techniques is tenuous, because the potential for morbidity increases; however, animal studies have shown that the spinal cord can tolerate higher doses if the length irradiated is 1 cm or less (13, 14). Because of its ability to deliver a highly focused dose, stereotactic irradiation can play a role in the treatment of these patients. Stereotactic irradiation is used effectively to treat intracranial lesions. Local control rates 82–99% were observed for 1,281 brain metastases in 10 reported series from radiosurgery centers around the world (15).

Linear accelerator (LINAC) technology and stereotactic hardware have advanced to the point where accurate stereotactic radiosurgery (SRS) and stereotactic radiotherapy (SRT) of the spine are possible. The transfer of stereotactic guidance technology from its traditional role as a targeting aid for intracranial lesions to a guide for irradiation of spinal lesions will increase the targeting accuracy and radiation dose conformation to tumors treated currently and will offer the opportunity to target tumors not formerly treatable. Increased targeting accuracy and dose conformation have the potential to reduce morbidity and patient discomfort while improving tumor response, duration of palliation, and quality of life. Accuracy is particularly important considering the close proximity of targets to the radiosensitive spinal cord. The first radiosurgery of the spine was reported by Hamilton *et al.*, who used a surgical approach for vertebral fixation and localization of spinal neoplasms (16). After treating nine patients, they concluded that spinal radiosurgery is technically feasible for the control of metastatic malignancies in the vertebral column (17). Murphy *et al.* reported the use of a robotic image-guided radiosurgical system to treat lesions in the spine, noting that implanted

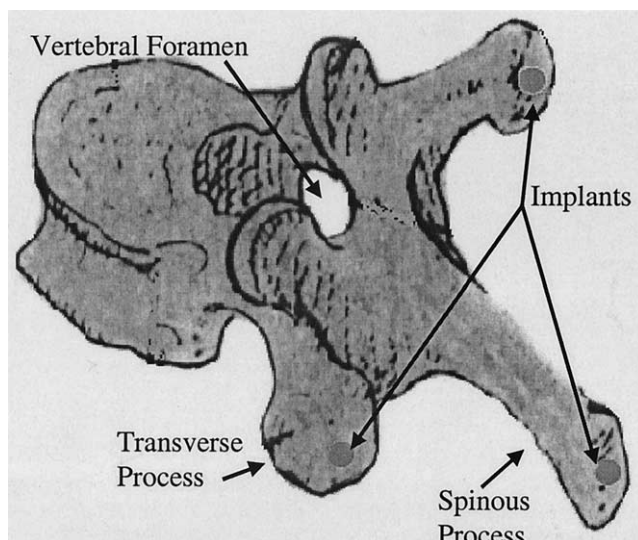


Fig. 1. Vertebra with three implants.

markers were used to provide radiographic landmarks for targeting in the thoracic spine (18).

METHODS AND MATERIALS

Method pursued

The spinal stereotactic radiotherapy (SSRT) procedure begins with the implantation of small ($1.7 \times 1.7 \times 2.1$ mm) titanium markers into the spinous and transverse processes of a vertebra (Fig. 1). Implants serve as fixed landmarks that are easily identified in standard diagnostic radiographs. When a minimum of three implants have been placed, a rigid body can be mathematically defined on the vertebra, and every point in the vertebra can be determined relative to the implanted markers. As applied to SSRT, if a target is chosen on an implanted vertebra, its location can always be recalculated, regardless of motion, as long as the coordinates of the three implants are known. The concept of incorporating implants for localization purposes is used presently in intracranial and extracranial SRT (18–20).

The implant procedure, performed under fluoroscopic guidance, is minimally invasive. With a patient in the prone position, a piercing stylet is inserted through a cannula, and the pair is pushed through the skin to a vertebral process. When a satisfactory position is attained, the cannula is held firmly against the bone surface, and the stylet is withdrawn. A drill tool is inserted through the cannula to the bone surface, and a shallow hole (2.5 mm deep) is turned by hand. The drill tool is withdrawn while the cannula continues to be held against the bone surface. An implant is threaded to the end of an applicator tool, and the applicator is inserted through the cannula to the bone surface. The implant is hand tapped into the drilled hole and left in the bone by twisting the applicator in the counterthread direction. The implant applicator and cannula are withdrawn from the patient to end the procedure.

After the placement of implants, a CT series and standard

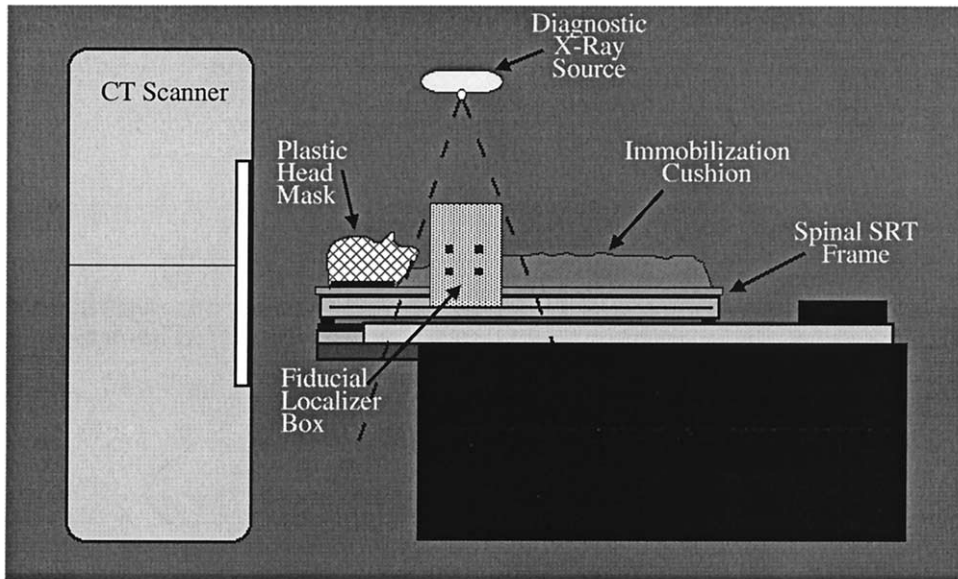


Fig. 2. SSRT imaging before treatment planning. A CT scan provides anatomic information for treatment planning and target selection, whereas concurrent biplanar radiographs are used to determine implant coordinates. Immobilization devices may be used to restrict patient motion.

biplanar radiographs are taken concurrently so that tumor and implant coordinates can be determined relative to one another. A coordinate system is defined during imaging procedures by an external SSRT frame (Fig. 2); a localization box that surrounds the patient contains both CT and plane film radiographic fiducial markers to provide a reference frame for coordinate determination (Fig. 3). Commercially available immobilization devices will be used for patient treatment, but were not included in this study. The CT scan provides anatomic information for treatment planning and target selection, whereas the radiographs are used to determine implant coordinates. Using CT and biplanar

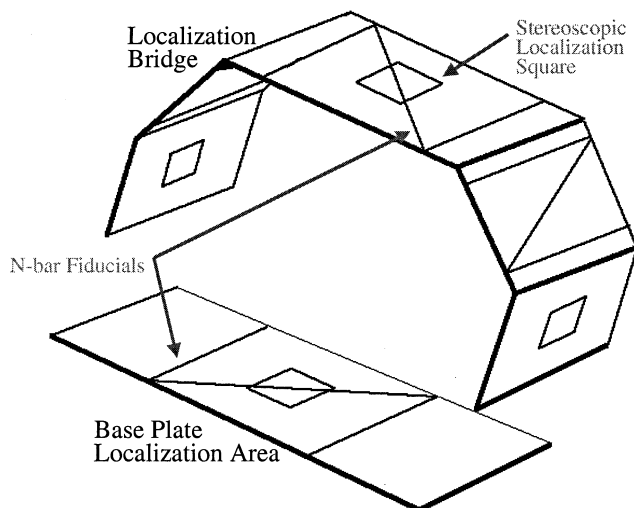


Fig. 3. SSRT localization box. N-bar fiducials are analogous to those used in the Brown-Roberts-Wells cranial-based SRS CT localization cage. Four markers on each face of the localization box are used for the stereoscopic localization of spinal implants.

radiographs for localization is common in intracranial SRS, and both localization techniques have been described in detail by other authors (21, 22). Stereoscopic localization (also called Roentgen stereophotogrammetry) is preferred for implant localization, because it is more accurate than CT, particularly when considering small targets in large fields of view.

As is standard in SRS procedures, a treatment plan is created after the CT imaging study. Once three implant positions have been determined, and a target has been chosen, a rigid body algorithm is used to define a target vector from the implants to the target. After a target vector has been established, the target position can always be calculated, regardless of vertebral orientation, as long as the implant positions are known. Gall *et al.* have described the process used in this research for defining a rigid body and creating a target vector from internal markers (20).

For the final step of the SSRT process, the patient is repositioned on the SSRT frame that is rigidly attached to the LINAC treatment couch (Fig. 4). Patient position is approximately the same as in the CT scan, but not necessarily identical. Biplanar radiographs are taken and analyzed for stereoscopic localization of implants. The target vector is applied to the rigid body defined by the implants, and an absolute target coordinate is calculated. The target is translated to the LINAC isocenter by aligning indexing marks on the SSRT frame with standard wall-mounted lasers. Radiation is delivered in a series of noncoplanar arcs or static conformal fields, depending on tumor size and shape.

Swine study

In accordance with the UCLA Chancellor's Animal Research Committee, a swine model was implemented to

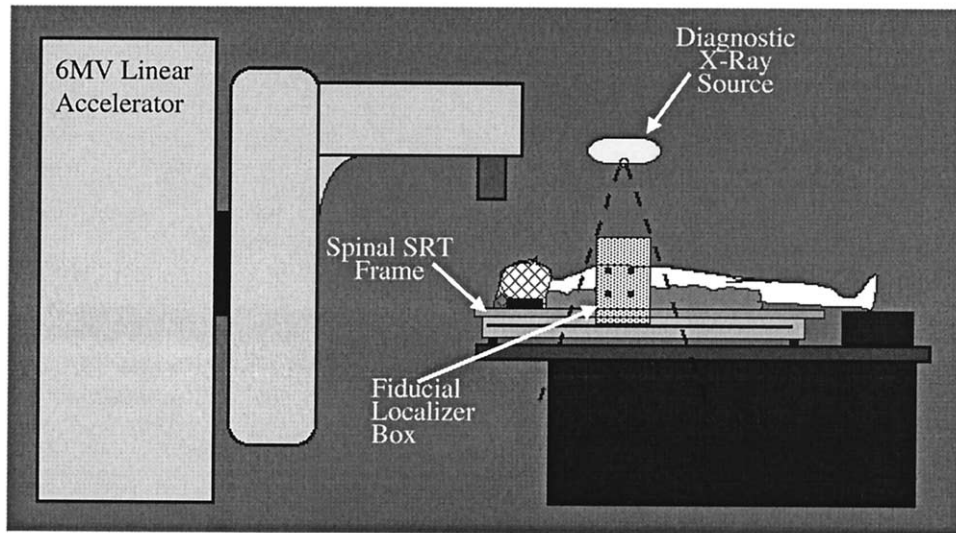


Fig. 4. SSRT LINAC setup. Anterior and lateral radiographs are exposed, using a standard mobile radiographic unit in the LINAC room.

assess the efficacy of the implant procedure and the use of spinal implants for radiation targeting. The swine study included four objectives. The first objective was to determine the duration and difficulty of the implant placement procedure. Although the use of spinal implants has been reported for orthopedic studies, a new style of implant and implant procedure was believed to be more appropriate for our study (23, 24). The second objective was to determine if the bone of the vertebral processes provides a suitable anchor for the implants such that the implants do not migrate over a period of 5 weeks. Third, there was concern that, although patients would be treated in the supine position, normal respiratory motion could cause the spine to move, resulting in a compromise of localization accuracy. Finally, the potential for using implants to target adjacent vertebrae was evaluated.

For the live animal in the swine study, the implant procedure was repeated nine times in one session. The swine was sedated, and titanium implants were placed in each vertebral process of one lumbar and two adjacent thoracic vertebrae. To determine implant coordinates, four stereoscopic imaging sessions (described further in the imaging section) were completed over a period of 5 weeks at 0, 18, 28, and 35 days postimplantation. Imaging studies were performed with the swine in the supine position and adjusted so that the implanted vertebra was in approximately the center of the localization box (Fig. 3). Radiograph pairs were approximately orthogonal, but varied up to $\pm 5^\circ$. All radiograph pairs were independently analyzed 10 times with in-house software and a Numonics backlit digitizer operating at 400-lines-per-centimeter resolution. An independent analysis consisted of affixing anterior-posterior (AP) and lateral film pairs to the digitizer and entering the positions of 8 stereoscopic fiducials and 3 implanted markers for each view.

Vertebral motion due to respiration was evaluated in two

ways. Stereotactic radiographs of implanted markers were exposed during full inhalation and exhalation phases and compared during film analysis. Implanted markers were also examined for motion under continuous fluoroscopy during full respiratory cycles.

Relative movement between adjacent vertebrae due to repositioning was investigated in the two implanted thoracic vertebrae. The three implants of the rostral thoracic vertebrae were used as targeting markers, whereas the three implants of the caudal vertebrae were used as easily identifiable targets. Target vectors to the three caudal implants were defined using the implant positions determined the day of implantation. The target vectors were applied in subsequent localization studies on Days 18, 28, and 35 to predict the locations of caudal implants given the rostral implant positions. The targeting error caused by intervertebral movement was determined as the distance between predicted and actual implant locations calculated using Eq. 1. No attempt was made to position the swine in the same way from day to day.

$$\text{Separation} = \sqrt{(x_1 - x_2)^2 + (y_1 - y_2)^2 + (z_1 - z_2)^2}, \quad (1)$$

where x , y , and z correspond to the AP, lateral, and axial coordinates of each point.

Theoretic targeting uncertainty

The use of implanted markers and the "rigid body" approach to localization has inherent limitations: Uncertainty in the location of each marker is translated into uncertainty in the target vector that points to the tumor/isocenter. Several groups have reported on the accuracy of the stereoscopic localization method, with a largest reported error of 0.5 mm (21, 25, 26). A treatment simulation program was written to study the propagation of uncertainty to the target

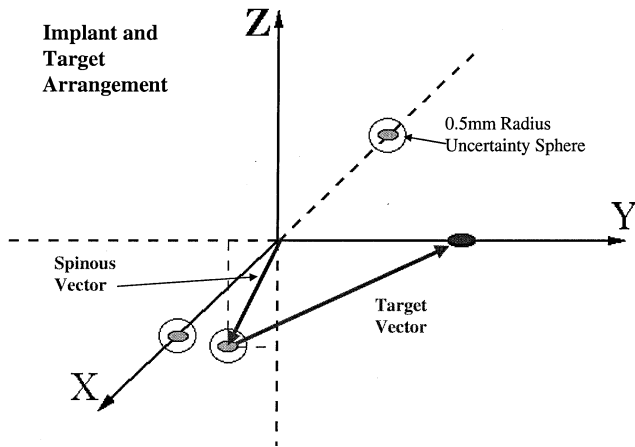


Fig. 5. Depiction of implant/target arrangement used in uncertainty simulation. Ovals on the x axis represent implants in the transverse processes; “transverse separation” is simply the distance between these two implants. The spinous vector points from the coordinate system origin (the point midway between the transverse process implants) to an implant in the spinous process. The target vector points from the spinous implant to a target (isocenter). Circles around implants indicate a sphere of uncertainty inherent in the stereoscopic localization process.

vector from the uncertainty inherent in the stereoscopic localization method. The simulation program uses a random number generator to assign implant locations within a 0.5-mm-radius error sphere centered on a true implant position. A target vector is calculated using three randomly displaced implants and then compared to a true target vector. Dimension measurements were taken from a model spine to estimate a range of clinically relevant implant/target configurations. Figure 5 provides a description of how implants are set up in software. The 1,400 implant/target configurations investigated included permutations of the following setup parameters: spinous process vector lengths 31, 22, 18, and 14 mm; transverse separations 10–80 mm; and target vector lengths 26–73 mm. Uncertainty distributions were tallied from 500K treatment histories for each of a variety of clinically relevant implant configurations. The mean, standard deviation, and 95% confidence interval were recorded from the uncertainty distributions.

Practical targeting uncertainty

Because of the reliance of the implant targeting method on accurate and precise stereoscopic localization, rigorous testing was performed on a prototype SSRT frame to evaluate its localization characteristics. Three plastic phantoms were used to evaluate the precision, relative accuracy, and targeting error inherent in the prototype frame. In particular, it was necessary to verify theoretic accuracy calculations to assure that the use of implants for localization is acceptable.

Precision of stereoscopic localization

To study the localization reproducibility of the fiducial localization box (Fig. 3), four plastic phantoms (Fig. 6) were made. A 1-mm-diameter steel chip embedded in each phan-

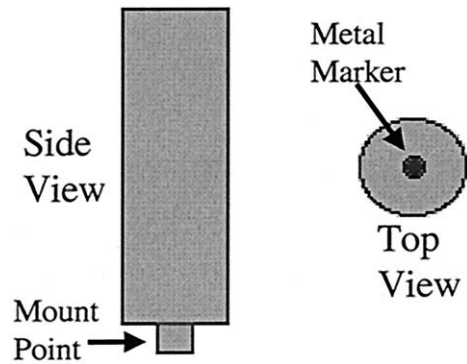


Fig. 6. Precision phantom. The mount point is inserted into holes on the surface of the spinal frame. The 1.0-mm-diameter metal marker is easily detected in radiographs.

tom was easily identified in diagnostic radiographs. The four precision phantoms were inserted into mounting points in the localization frame and stereoscopically radiographed three times. Each radiograph pair was exposed with a 0.6-mm focal spot at random source/frame angles $\pm 5^\circ$ from orthogonal with a standard radiation therapy simulator. Source-to-film distance was 100 ± 10 cm. Radiograph pairs were approximately orthogonal, but allowed to vary up to $\pm 10^\circ$. All radiograph pairs were independently analyzed 10 times with in-house software and a Numonics backlit digitizer operating at 400-lines-per-cm resolution. An independent analysis consisted of fixing AP and lateral film pairs to the digitizer and entering the positions of the 8 stereoscopic fiducials and 4 phantom markers for each view. Thus, the position of each precision phantom was calculated and recorded 30 ($= 3 \times 10$) times.

Upon completion of this study, mean AP, lateral, and axial coordinates were calculated from the 30 measurements of each phantom position. The three-dimensional distance from the mean phantom location to each individual measurement was calculated using Eq. 2, and a mean and standard deviation were calculated from the resulting distribution.

$$3D \text{ Dist.} = \sqrt{(X - \bar{X})^2 + (Y - \bar{Y})^2 + (Z - \bar{Z})^2}, \quad (2)$$

where \bar{X} , \bar{Y} , and \bar{Z} are distribution means.

Relative accuracy of stereoscopic localization

The second practical localization study performed incorporated a distance-measuring phantom (Fig. 7) to determine the spinal frame's relative localization accuracy. The distance phantom secures two steel pointers that can be extended and retracted to vary the point-to-point separation. Point-to-point separation was physically measured with a dial caliper and compared to localization calculations.

Radiographic setup and analysis conditions were identical to those of the precision study. In three independent trials, the distance phantom was placed in a random orientation in the central area of the localization frame. For each

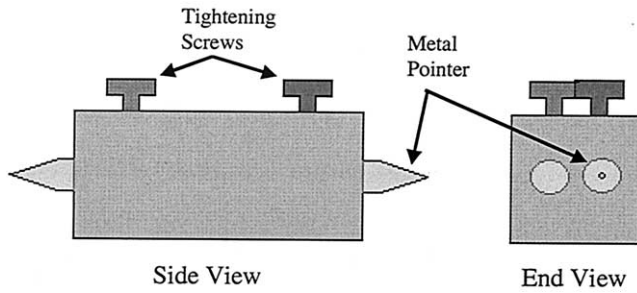


Fig. 7. Distance phantom. Steel pointers can be extended and retracted to vary the point-to-point distance. Tightening screws lock the pointers in place. Point-to-point distance ranges from 5.5 cm to 13 cm. Steel pointers taper from a 6-mm diameter to a fine point that is identified on standard stereoscopic radiographs.

trial, a random point-to-point distance was set, and one stereoscopic pair of radiographs was exposed. Each radiograph pair was independently analyzed 10 times to calculate point positions. The distance between points was calculated according to Eq. 1.

Targeting error using localized implants to define a rigid body

Two studies were performed with a vertebral phantom (Fig. 8). The vertebral phantom is designed to approximate the dimensions of potential target/implant arrangements. A series of titanium vertebral implants are embedded in holes drilled through the surface of each phantom arm, so many target/implant combinations can be investigated simultaneously. The first vertebral phantom study was similar to the precision phantom study already discussed, except actual implants were localized instead of the smaller steel chips. The second study was an investigation of target vector uncertainty to confirm theoretic uncertainty calculations.

In the first study, the vertebral phantom was loaded with 16 implants and stereoscopically radiographed in two random orientations. Each pair of radiographs was independently analyzed 11 times using the same radiographic and analytic techniques described for the precision study. For each implant, a mean position was calculated from the 11 samples. The three-dimensional distances from the mean positions to all 176 ($= 16 \times 11$) individual samples were calculated according to Eq. 2, and a mean and standard deviation were calculated from the resulting distribution.

The second vertebral phantom study was designed to measure targeting error. By using actual spinal implants in clinically relevant arrangements, this study was intended to simulate clinical situations and to confirm the theoretic uncertainty calculations discussed earlier. A wide range of configurations was studied to include all conceivable clinical situations, from small vertebrae with tight implant groupings to large vertebrae with relatively spacious implant groupings. The vertebral phantom was loaded with 19 titanium implants, so uncertainty could be evaluated for a potential range of 500 ($= 5 \times 5 \times 4 \times 5$) implant/target combinations. Implants were distributed with 5 in each

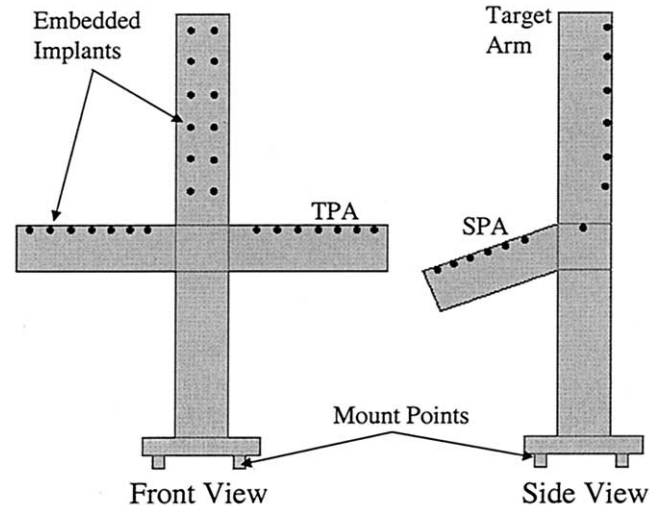


Fig. 8. Vertebral phantom. The four arms of the phantom simulate a vertebra (target arm, right and left transverse process arms [TPA], and a spinous process arm [SPA]). A series of implants is embedded in each arm, so many implant combinations can be investigated. Mount points can be inserted into holes on the surface of the spinal frame to simulate a patient in the supine position, or the phantom can be laid in any random orientation. The transverse process arms are 8 cm from end to end. The target arm rises 6.5 cm above the transverse process arms. The spinous process arm extends 3.5 cm from the transverse process arms.

transverse process arm, 4 in the spinous process arm, and 5 in the target arm (Fig. 8). The phantom was stereoscopically radiographed in 37 random orientations in the central localization region. Radiographic and digitization conditions were the same as for the precision study. All implants were digitized only once for each pair of radiographs, except for the implants in the target arm, which were digitized three times. The mean of the three independent localizations was assumed to be the true location of each target arm implant. Using the standard deviation observed in the vertebral phantom precision study (0.04 mm), a sample size of three resulted in a confidence interval of ± 0.05 mm with a 95% confidence level (Eq. 3). Thirty-seven trials (pairs of radiographs) were completed, so that an estimate of the population mean could be calculated with reasonable certainty. The number of trials necessary was calculated according to the following common statistics formula (Eq. 3):

$$n = \frac{(z_{\alpha/2})^2 \sigma^2}{E^2}, \quad (3)$$

where n is the required sample size, σ is the population standard deviation, E is the width of the confidence interval (e.g., $E = 0.1$ indicates the sample mean will be ± 0.1 of the true mean), and $z_{\alpha/2}$ is the confidence level value (the value of a normal curve such that the upper-tail area is $\alpha/2$ when the $100[1 - \alpha]\%$ confidence level is desired; e.g., $z = 1.96$ for the 95% confidence level) (27).

For the target vector error study, the appropriate standard

Table 1. Variability of implant localization in swine vertebrae (mm)

Day	Mean	Standard deviation	Minimum	Maximum
0	0.06	0.04	0.01	0.24
18	0.07	0.04	0.01	0.18
28	0.07	0.05	0.01	0.25
35	0.07	0.04	0.01	0.20

deviations were estimated from the theoretic uncertainty results to range from 0.2 to 0.6 mm, depending on the implant configuration. A 95% confidence level was chosen, so $z = 1.96$. The number of trials (radiograph pairs) was fixed at 37, so the confidence interval varied from ± 0.06 mm to ± 0.19 mm, depending on the implant configuration in question.

After positions were calculated for all 19 implants, local coordinate systems were defined on the phantom. Target vectors for all implant/target combinations were calculated from the first radiograph pair and applied in the subsequent 36 radiograph pairs to calculate expected target coordinates for all implant combinations. The expected target coordinates were compared to target coordinates measured from the vertebral phantom, and differences were recorded. Distributions of target uncertainty were tabulated for 100 implant/target arrangements. In all, 1,073 ($= 29 \times 37$) implants were localized, 1,776 ($= 48 \times 37$) fiducial markers were digitized, and 3,600 ($= 36 \times 100$) pairs of target coordinates were compared in the target vector uncertainty study.

RESULTS

Swine study

The implant procedure was expedient, at 5–10 minutes per site. No complications were experienced, and the swine exhibited normal behavior after implantation. Blood loss was negligible, and skin puncture wounds were nearly invisible at 35 days post procedure.

In the four imaging sessions after implantation (Days 0, 18, 28, and 35), the mean anterior-posterior, lateral, and axial coordinates of all nine implants were calculated after analyzing each radiograph pair 10 times. The distance from the mean implant location to each individual measurement was calculated using Eq. 2, and a distance distribution was recorded. Results of the distance distributions by imaging session are presented in Table 1. Each reported mean, standard deviation, minimum, and maximum is the result of 90 measurements ($3 \text{ implants} \times 3 \text{ vertebrae} \times 10 \text{ analyses}$). There was concern that the precision of the localization process in the swine would suffer compared to simpler phantom measurements; however, precision was almost identical.

No attempt was made to align the swine in exactly the same position from one imaging session to the next, so absolute implant positions cannot be compared. Instead, the

Table 2. Implant separations in vertebra (mm)

2a. Rostral thoracic			
Rostral thoracic vertebra			
Day	Rt to Lt trans	Rt trans to spin	Lt trans to spin
0	26.58	26.78	23.45
18	26.46	26.79	23.78
28	26.73	26.96	23.73
35	26.51	26.81	23.64
2b. Caudal thoracic			
Caudal thoracic vertebra			
Day	Rt to Lt trans	Rt trans to spin	Lt trans to spin
0	31.31	23.19	24.38
18	30.78	23.06	24.73
28	30.90	23.33	24.50
35	30.65	23.42	24.43
2c. Lumbar			
Lumbar vertebra			
Day	Rt to Lt trans	Rt trans to spin	Lt trans to spin
0	64.66	34.86	40.03
18	65.32	34.54	40.02
28	65.64	34.81	40.06
35	65.93	34.96	39.94

Abbreviations: Rt = right; Lt = left; Trans = transverse; Spin = spinous.

relative separation between implants is used as a measure of implant migration. The implant separations were calculated using Eq. 1 and are reported separately for each vertebra in Tables 2a–c. Separation data for the rostral thoracic vertebra (Table 2a) are very consistent. The largest range from minimum to maximum separation for any two implants was 0.33 mm. Separations for the caudal thoracic vertebra were unremarkable, except for the transition from Day 0 to Day 18, where the right-to-left transverse process distance decreased by 0.53 mm. At the same time, the left transverse to spinous process distance increased by 0.35 mm. The greatest separation differences were observed in the lumbar vertebra. The right-to-left transverse process distance increased each day at a nearly constant rate of 0.04 mm/day, suggesting a growth pattern. Separations from the spinous process to the transverse processes varied about the same as

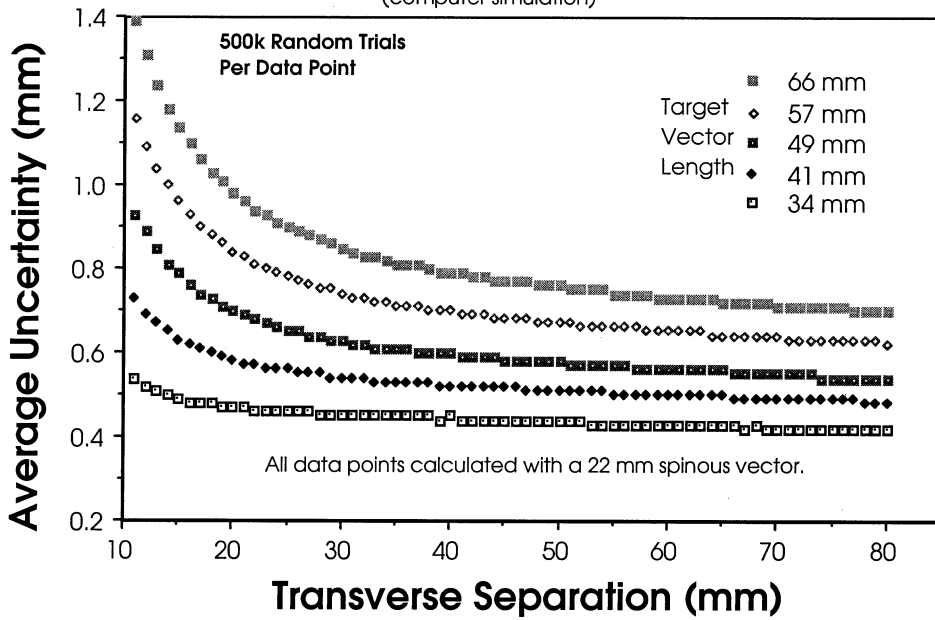
Table 3. Error when a thoracic vertebra is used to target an adjacent vertebra (mm)

Target location			
	Rt trans process	Spinous process	Lt trans process
Day 18	0.71	0.60	1.37
Day 28	1.17	0.85	1.43
Day 35	1.54	1.19	1.41

Abbreviations: Rt = right; Lt = left; Trans = transverse.

Average Uncertainty vs. Implant Separation

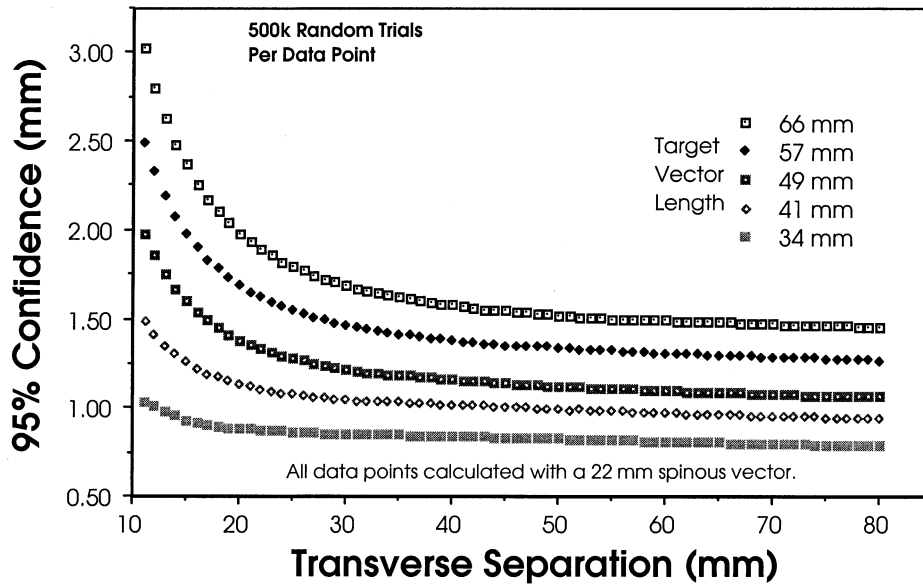
(computer simulation)



(a)

95% Confidence Uncertainty vs. Implant Separation

(computer simulation)



(b)

Fig. 9. (a) Average theoretic uncertainty. Various clinically relevant implant configurations were investigated to determine the average random uncertainty inherent in the rigid body targeting method. This figure shows the targeting uncertainty of implant arrangements that include a 22-mm spinous vector; the transverse separation and target vector lengths are varied. Standard deviation varies according to target vector length and transverse separation. As transverse separation increases from 10 mm to 80 mm, standard deviation ranges are as follows: 0.84–0.39 mm, 0.69–0.34 mm, 0.54–0.28 mm, 0.40–0.24 mm, and 0.27–0.20 mm, respectively, for target vector lengths of 66 mm, 57 mm, 49 mm, 41 mm, and 34 mm. Averages are generated using a computer simulation with 500K samples per implant configuration (See Fig. 5 for definitions of target vector length, spinous vector, and transverse separation). (b) Theoretic 95% confidence level. Various clinically relevant implant configurations were investigated to determine the random uncertainty inherent in the rigid body targeting method. This figure shows the targeting uncertainty of implant arrangements that include a 22-mm spinous vector; the transverse separation and target vector lengths are varied. In a computer simulation, 500K samples of random target vector uncertainty were taken for each implant configuration; 95% of samples were less than or equal to the values shown (See Fig. 5 for definitions of target vector length, spinous vector, and transverse separation).

in the thoracic vertebrae. With the exception of the right-to-left transverse separations of the caudal thoracic and lumbar vertebrae, the largest range from minimum to maximum separation for any two implants from any vertebra was 0.42 mm.

Respiration did not cause any detectable implant motion in either the fluoroscopic or plane film studies. Inhalation and exhalation radiographs were interchangeable for analysis. "Adjacent vertebra" targeting error by day is presented in Table 3. Error for targeting an adjacent vertebra was smaller than expected, but always larger than in theoretic and phantom studies for "same vertebra targeting" with similar implant arrangements. Target vector lengths (Fig. 5) were 32.9, 21.1, and 35.7 mm for targets in the right transverse, spinous, and left transverse processes, respectively. The spinous vector length was 21.4 mm, and transverse separation was 26.6 mm. None of the theoretic or phantom implant arrangements investigated match these dimensions exactly, but uncertainties can be approximated by interpolation. The maximum targeting error in the vertebral phantom study for a 28-mm transverse separation, 22-mm spinous vector, and 34-mm target vector was 0.43 mm (Table 6b). The mean and 95% confidence level for the same setup are 0.46 and 0.86 mm by theoretic calculations (Figs. 9a and 9b).

Theoretic targeting uncertainty

More than 1,400 implant/target configurations have been investigated to determine the average and 95% confidence levels of target vector uncertainty. For the sake of brevity, the average and 95% confidence levels of only a sample of implant/target configurations are presented (Figs. 9a and 9b). Phantom measurements made to verify the theoretic calculations are presented later.

Practical targeting uncertainty

Precision of stereoscopic localization. The means and standard deviations of localization variation in the central area of the localization box are presented in Table 4. Each reported mean and standard deviation is the result of 10 radiograph analyses. The mean and standard deviation for all 120 trials (4 phantoms \times 3 film pairs \times 10 analyses) is 0.08 ± 0.04 mm. The minimum and maximum deviation from the mean for all 120 trials was 0.02 mm and 0.23 mm, respectively.

Table 5. Relative localization accuracy (mm)

	Calculated value				Measured value
	Mean	SD	Minimum	Maximum	
Trial 1	56.20	0.08	56.10	56.31	56.26
Trial 2	78.18	0.05	78.10	78.26	78.26
Trial 3	69.76	0.09	69.62	69.92	69.72

Abbreviation: SD = standard deviation.

The precision phantom study established the variability of the stereoscopic localization procedure on our SSRT frame. The theoretic error study (Figs. 9a and 9b) incorporated a 0.5-mm-diameter error sphere around each implant, but this practical study suggests a sphere of radius 0.23 mm may be more appropriate. As Table 4 shows, a mean <0.1 mm and maximum variability of 0.23 mm were achieved for localization in the central region. In addition, no significant differences were found between measurements from differing film pairs or phantoms.

Relative accuracy of stereoscopic localization. A distance-measuring phantom of known length (Fig. 7) was radiographed and the length calculated from localization results of the two points. The results of physical measurements vs. phantom lengths calculated from localization results are presented in Table 5. Numbers reported in Table 5 are the result of 10 film analyses of each phantom configuration. Average stereoscopic measurements of length were within 0.1 mm of physical caliper measurements, and a maximum range of 0.3 mm was observed over the 10 stereoscopic measurements of the same phantom length. Variation in the stereoscopic length measurements is a consequence of the variation in each point location used to calculate length.

Targeting error using localized implants to define a rigid body. To verify theoretic calculations of targeting error, physical measurements of error were made using a vertebral phantom (Fig. 8). The 100 implant/target configurations investigated include permutations of the following setup parameters: spinous process vector lengths of 31, 22, 18, and 14 mm; transverse separations of 76, 52, 44, 36, and 28 mm; and target vector lengths from 26 to 73 mm. For the sake of brevity, the mean, standard deviation, and minimum and maximum observed targeting errors are presented for only 25 implant/target configurations (Table 6a, 6b). Con-

Table 4. Variability (mm) from the mean position for localization in the central region

Phantom	Film pair 1		Film pair 2		Film pair 3		All films	
	Mean	SD	Mean	SD	Mean	SD	Mean	SD
A	0.08	0.04	0.07	0.02	0.07	0.05	0.08	0.04
B	0.12	0.05	0.07	0.03	0.08	0.04	0.09	0.04
C	0.09	0.03	0.09	0.03	0.07	0.03	0.08	0.03
D	0.09	0.04	0.08	0.03	0.08	0.02	0.08	0.03

Abbreviation: SD = standard deviation.

Table 6a. Mean uncertainty (in mm) for implant arrangements with a 22-mm spinous vector length

Tran sep	Targ vect 1*		Targ vect 2		Targ vect 3		Targ vect 4		Targ vect 5	
	Mean	SD	Mean	SD	Mean	SD	Mean	SD	Mean	SD
76	0.24	0.12	0.19	0.10	0.23	0.10	0.19	0.09	0.19	0.08
52	0.39	0.18	0.34	0.14	0.40	0.12	0.34	0.08	0.30	0.09
44	0.29	0.14	0.23	0.11	0.30	0.12	0.25	0.08	0.22	0.08
36	0.36	0.15	0.29	0.13	0.36	0.12	0.30	0.09	0.28	0.08
28	0.28	0.15	0.23	0.13	0.29	0.12	0.23	0.09	0.21	0.09

Table 6b. Minimum and maximum uncertainty (in mm) for implant arrangements with a 22-mm spinous vector length

Tran sep	Targ vect 1*		Targ vect 2		Targ vect 3		Targ vect 4		Targ vect 5	
	Min	Max	Min	Max	Min	Max	Min	Max	Min	Max
76	0.06	0.63	0.03	0.48	0.02	0.45	0.03	0.39	0.05	0.38
52	0.14	0.94	0.14	0.74	0.21	0.67	0.22	0.58	0.16	0.53
44	0.10	0.71	0.06	0.55	0.05	0.51	0.09	0.44	0.09	0.41
36	0.09	0.85	0.09	0.69	0.10	0.67	0.14	0.49	0.13	0.49
28	0.10	0.78	0.09	0.61	0.10	0.59	0.10	0.42	0.08	0.43

* Target vector lengths are 66, 49, 41, and 34 mm for target vectors 1–5, respectively.

Abbreviations: Tran sep = transverse separation; Targ vect = target vector; SD = standard deviation; Min = minimum; Max = maximum.

figurations are identical to those reported for the theoretic study (Figs. 9a and 9b), so results may be compared directly.

Comparison of Tables 6a and 6b with Figs. 9a and 9b shows a substantial difference between the theoretic computer-generated target vector uncertainties and practical measurements. Over the 100 implant/target configurations studied, theoretic means ranged from 1.5 to more than 3 times larger than the corresponding values measured with the vertebral phantom. Theoretic 95% confidence level values were also 1.5 to more than 3 times the measured maximums. The largest targeting error observed for any of the 100 implant configurations studied was 1.17 mm. The smaller-than-theorized uncertainties are not surprising when the results of the vertebral phantom variability study are considered (Table 7). The largest single implant deviation observed in the variability study was 0.23 mm, but theoretic uncertainty calculations are based on a maximum deviation of 0.5 mm.

A second series of theoretic calculations was performed, incorporating a reduced uncertainty sphere with 0.25-mm radius. All program parameters used were identical to the initial study, except for the reduction in the uncertainty sphere radius. The second theoretic series investigated only implant/target arrangements with 22-mm spinous vector

lengths. Results of the secondary study are presented in Tables 8a and 8b. Comparison of Table 8a and Fig. 9a shows good agreement between practical measurements and theoretic calculations. Theoretic uncertainty calculations overestimated the mean for 16 of the 25 implant/target arrangements by an average of 0.07 mm. The remaining 9 arrangements were underestimated by an average of only 0.05 mm. The maximum overestimation and underestimation was 0.12 mm and 0.11 mm, respectively. Standard deviation was overestimated for all 25 arrangements by an average of 0.04 mm. The theoretic 99% confidence levels (Table 8b) were greater than all measured maximums by an average of 0.18 mm, with one exception that was underestimated by 0.02 mm. Theoretic calculations are based on 500K trials, compared to 37 practical measurements per data point; deviations of the measured data from the theoretic data are likely a consequence of the relatively low number of measurements. Deviations of the sample means for 37 trials fell within the expected confidence interval as calculated by Eq. 3.

DISCUSSION

The use of internal implants to target spinal malignancies for LINAC stereotactic irradiation has been investigated in preparation for clinical trials. The implant procedure was implemented on swine, and evaluations of the theoretic and practical limitations of localization accuracy were performed using a computer simulation of the targeting procedure and using phantom measurements.

Although resources limited the animal study to one live and two postmortem swine, fundamental questions were answered regarding the potential for use of implanted spinal

Table 7. Implant localization variability (mm)

Phantom position	Mean	SD	Minimum	Maximum
Orientation 1	0.07	0.04	0.01	0.23
Orientation 2	0.05	0.03	0.01	0.14

Abbreviation: SD = standard deviation.

Table 8a. Mean uncertainty (in mm) for implant arrangements with a 22-mm spinous vector length

Tran sep	Targ vect 1*		Targ vect 2		Targ vect 3		Targ vect 4		Targ vect 5	
	Mean	SD	Mean	SD	Mean	SD	Mean	SD	Mean	SD
76	0.35	0.20	0.31	0.17	0.27	0.14	0.24	0.12	0.21	0.10
52	0.37	0.20	0.33	0.18	0.29	0.15	0.25	0.13	0.22	0.10
44	0.39	0.21	0.34	0.18	0.29	0.15	0.26	0.13	0.22	0.11
36	0.40	0.21	0.36	0.19	0.30	0.15	0.26	0.13	0.22	0.11
28	0.43	0.23	0.38	0.20	0.32	0.16	0.27	0.14	0.23	0.11

Table 8b. 99% confidence level (in min) for implant arrangements with a 22-mm spinous vector length

Tran sep	Targ vect 1* (99% CI)	Targ vect 2 (99% CI)	Targ vect 3 (99% CI)	Targ vect 4 (99% CI)	Targ vect 5 (99% CI)
76 mm	0.95	0.82	0.69	0.60	0.49
52 mm	0.97	0.84	0.71	0.62	0.51
44 mm	0.99	0.86	0.72	0.63	0.52
36 mm	1.02	0.89	0.74	0.64	0.53
28 mm	1.08	0.94	0.78	0.66	0.53

* Target vector lengths are 66, 57, 49, 41, and 34 mm for target vector 1–5, respectively.

Abbreviations: Tran sep = transverse separation; Targ vect = target vector; SD = standard deviation; CI = confidence interval.

markers. Implanted markers were readily distinguishable from normal anatomy on radiographs, allowing a localization variance similar to phantom studies and suggesting that an autodetection algorithm may be usable to expedite the targeting process. The swine study suggests that it may be reasonable to use implanted markers to target adjacent vertebrae with a small sacrifice in accuracy. It is believed that the targeting error seen in this study could be reduced if mature swine and a repositioning device were used. The swine used in this study grew from 29 kg to an estimated 36 kg in 5 weeks, contributing to the targeting error recorded; targeting error for adjacent vertebrae increased over time. Incorporation of an immobilization/repositioning device, such as a vacu-lock bag, may reduce flexion of the spine and better approximate a rigid body between vertebrae.

As expected, target vector uncertainty increases as implants are grouped closer together and as the target gets farther from the implants. Certain implant arrangements could produce unacceptable uncertainty as separation becomes too small or the target becomes too distant. Experience with spine models and our swine study suggests that reasonable separation is achievable by placing implants in the vertebral processes. For adults, it is believed transverse separations greater than 35 mm and target vectors around 50 mm will be common. Uncertainty simulations can be computed in minutes on an individual basis, so potential for

error can be assessed before irradiation begins. Deformation of the fiducial configuration because of marker migration or patient motion is an important issue in fiducial-based targeting. Deformation is largely an unknown in a clinical setting and will require the user to implement quality assurance measures to maximize accuracy.

It is recognized that the targeting error inherent in the presented localization technique is not the total application error of the SSRT procedure. Perhaps the major introduction of error in the SSRT procedure comes from the CT imaging, as is the case for CT-based intracranial SRS systems (28, 29). The SSRT system is not unique, because all SRT systems suffer from the localization inaccuracies of either CT or MRI. The purpose of these initial SSRT studies was not to determine total application error, but rather to characterize the error suffered directly as a result of using implants for targeting. Imaging error aside, the error incurred in this SSRT technique is comparable to error suffered by intracranial SRT systems in their repositioning methods (30–32). An evaluation of application accuracy is under way.

The use of implanted markers for localization of spinal malignancies has potential for applications in stereotactic irradiation. Phantom measurements suggest that localization accuracy similar to intracranial stereotactic radiotherapy techniques is achievable.

REFERENCES

1. Malawer MM, Delaney TF. Treatment of metastatic cancer to bone. In: DeVita VT, Hellman S, Rosenberg SA, editors. *Cancer: Principles and practice of oncology*. Philadelphia: Lippincott; 1993. p. 2225–2245.
2. Clain A. Secondary malignant disease of bone. *Br J Cancer* 1965;19:15.
3. Bansal S, Brady LW, Olsen A, *et al.* The treatment of metastatic spinal cord tumors. *JAMA* 1967;202(8):686–688.
4. Grant R, Papadopoulos SM, Greenberg HS. Metastatic epidural spinal cord compression. *Neurol Clin* 1991;9(4):825–841.
5. Landmann C, Hunig R, Gratzl O. The role of laminectomy in

- the combined treatment of metastatic spinal cord compression. *Int J Radiat Oncol Biol Phys* 1992;24(4):627–631.
6. Gilbert RW, Kim JH, Posner JB. Epidural spinal cord compression from metastatic tumor: Diagnosis and treatment. *Ann Neurol* 1978;3(1):40–51.
 7. Tong D, Gillick L, Hendrickson FR. The palliation of symptomatic osseous metastases: Final results of the study by the Radiation Therapy Oncology Group. *Cancer* 1982;50(5):893–899.
 8. Sorensen S, Borgesen SE, Rohde K, *et al.* Metastatic epidural spinal cord compression. Results of treatment and survival. *Cancer* 1990;65(7):1502–1508.
 9. Maranzano E, Latini P. Effectiveness of radiation therapy without surgery in metastatic spinal cord compression: Final results from a prospective trial. *Int J Radiat Oncol Biol Phys* 1995;32(4):959–967.
 10. Gilbert HA, Kagan AR, Nussbaum H, *et al.* Evaluation of radiation therapy for bone metastases: Pain relief and quality of life. *Am J Roentgenology* 1977;129(6):1095–1096.
 11. Marcus RB Jr, Million RR. The incidence of myelitis after irradiation of the cervical spinal cord. *Int J Radiat Oncol Biol Phys* 1990;19(1):3–8.
 12. Schultheiss TE. Spinal cord radiation “tolerance”: Doctrine versus data. *Int J Radiat Oncol Biol Phys* 1990;19(1):219–221.
 13. Hopewell JW, Morris AD, Dixon-Brown A. The influence of field size on the late tolerance of the rat spinal cord to single doses of X rays. *Br J Radiol* 1987;60(719):1099–1108.
 14. van der Kogel AJ. Dose-volume effects in the spinal cord. *Radiother Oncol* 1993;29(2):105–109.
 15. Mehta M. Radiosurgery for brain metastases. In: De Salles AAF, Goetsch SJ, editors. *Stereotactic surgery and radiosurgery*. Madison, WI: Medical Physics Publishing; 1993. p. 353–364.
 16. Hamilton AJ, Lulu BA, Fosmire H, *et al.* Preliminary clinical experience with linear accelerator-based spinal stereotactic radiosurgery. *Neurosurgery* 1995;36(2):311–319.
 17. Hamilton AJ, Lulu BA, Fosmire H, *et al.* LINAC-based spinal stereotactic radiosurgery. *Stereotact Funct Neurosurg* 1996;66:1–9.
 18. Murphy MJ, Adler JR Jr, Bodduluri M, *et al.* Image-guided radiosurgery for the spine and pancreas. *Comput Aid Surg* 2000;5:278–288.
 19. Jones D, Christopherson DA, Washington JT, *et al.* A frameless method for stereotactic radiotherapy. *BJR* 1993;66:1142–1150.
 20. Gall KP, Verhey LJ, Wagner M. Computer-assisted positioning of radiotherapy patients using implanted radiopaque fiducials. *Med Phys* 1993;20(4):1153–1159.
 21. Siddon RL, Barth NH. Stereotaxic localization of intracranial targets. *Int J Radiat Oncol Biol Phys* 1987;13:1241–1246.
 22. Galloway RL, Maciunas RJ. Stereotactic neurosurgery. *Crit Rev Biomed Eng* 1990;18(3):181–205.
 23. Aronson AS, Holst L, Selvik G. *Radiology* 1974;113:733–734.
 24. Selvik G. Roentgen stereophotogrammetric analysis. *Acta Radiol* 1990;31:113–126.
 25. Vandermeulen D, Suetens P, Gybels J, *et al.* Angiographic localizer for the BRW stereotactic system. *Appl Neurophysiol* 1987;50:87–91.
 26. Friedman WA, Bova FJ. The University of Florida radiosurgery system. *Surg Neurol* 1989;32(5):334–342.
 27. Ott L. An introduction to statistical methods and data analysis. 3rd ed. Boston: PWS-Kent; 1988. p. 130–132.
 28. Winston KR, Lutz W. Linear accelerator as a neurosurgical tool for stereotactic radiosurgery. *Neurosurgery* 1988;22:454–464.
 29. Maciunas RJ, Galloway RL, Latimer JW. The application accuracy of stereotactic frames. *Neurosurgery* 1994;35:682–695.
 30. Murphy MJ, Cox RS. The accuracy of dose localization for an image-guided frameless radiosurgery system. *Med Phys* 1996;23(12):2043–2049.
 31. Bova FJ, Buatti JM, Friedman WA, *et al.* The University of Florida frameless high-precision stereotactic radiotherapy system. *Int J Radiat Oncol Biol Phys* 1997;38(4):875–882.
 32. Kooy HM, Dunbar SF, Tarbell NJ, *et al.* Adaption and verification of the relocatable Gill-Thomas-Cosman Frame in stereotactic radiotherapy. *Int J Radiat Oncol Biol Phys* 1994;30(3):685–691.